

Experimental study of the runner blade-to-blade shear flow turbulent mixing in the cone of Francis turbine scale model

Authors	Firm / Institution	City, Country	Lecturer (x)
Monica Sanda Iliescu Gabriel Dan Ciocan François Avellan	EPFL/LMH Swiss Federal Institute of Technology, Laboratory for Hydraulic Machines	Lausanne, Switzerland	x

Abstract

The runner blade-to-blade shear flow turbulent mixing characteristics in the cone of a Francis turbine scale model are investigated by using the 3D PIV Technique. From the experimental flow survey, the periodic component of the instantaneous velocity field is extracted by a phase averaging procedure. This procedure made apparent the main structures of the flow and the mixing process of the incoming shear flow.

Résumé

Le mélange turbulent du cisaillement de l'écoulement du canal aube-à-aube est étudié dans le cône d'un modèle réduit de turbine Francis par une technique de PIV 3D. La composante périodique du champ instationnaire de vitesse est extraite par une méthode de moyenne de phase à partir du relevé expérimental de l'écoulement. Cette méthode fait apparaître les structures principales de l'écoulement et le processus de mélange de l'écoulement cisailé incident.

Nomenclature

E	Specific Energy,	[J/Kg]	γ	Specific Energy Coefficient	[-]
Q	Discharge	[m ³ /s]	φ	Discharge Coefficient	[-]
Q_{BEP}	Flow Rate at the Best Efficiency Operating Condition	[m ³ /s]	n	Specific Speed	[-]
Re	Reynolds Number	[-]	ω	Rotational Pulsation	[rad/s]
D_{Te}	Runner Diameter	[m]	ΔZ	Cone Height	[m]
C_i	Instantaneous Velocity	[m/s]	\bar{C}	Time-Averaged Velocity Value	[m/s]
\bar{c}	Periodic Fluctuating Component	[m/s]	C'	Random Turbulent Fluctuation	[m/s]
C_u	Tangential Component	[m/s]	C_r	Circumferential Component	[m/s]
C_z	Axial Component	[m/s]	U	Peripheral Speed	[m/s]
C	Absolute Velocity	[m/s]	W	Relative Velocity	[m/s]
C_{ref}	Mean Flow Reference Velocity $C_{ref} = Q/A$	[m/s]	C_c	Runner Blades Wake Centerline Velocity Defect	[m/s]

L_c	Runner Blade Chord	[m]	L	Streamwise Distance	[m]
f	Runner Rotation Frequency	[Hz]	f_b	Blade Passing Frequency	[Hz]
τ	Peripheral Position of the Runner	[s]	z_b	Number of Runner Blades	[-]
T	Runner Rotation Period	[s]	T_b	Blade Passing Period	[s]

Introduction

The energy transfer within a turbine runner results in an uneven relative flow velocity distribution in the runner blade-to-blade channel of jet-wake type. Moreover, a turbulent wake at the blade trailing edge is originating from the boundary layer developments on both the high-pressure side and the low-pressure side of the runner blades. The superposition of the main uneven relative flow distribution with the turbulent wake of the blades stand at the origin of the flow non-uniformity at the cone inlet, and generates a sheared periodic flow in the draft tube cone, see Figure 1.

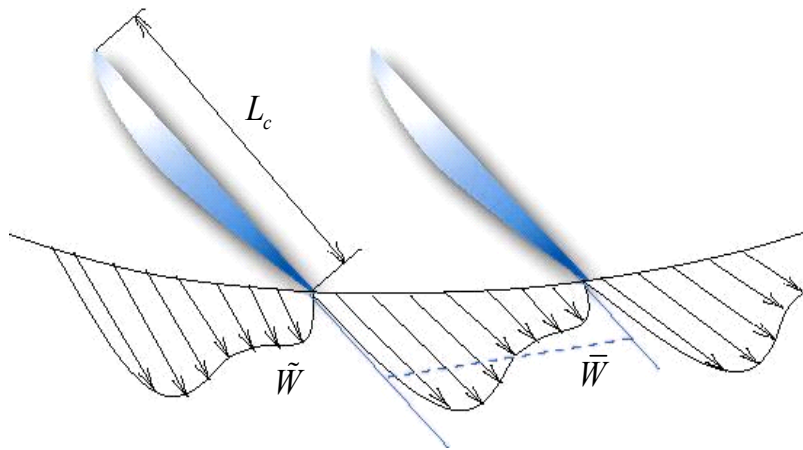


Figure 1 Blade to blade flow distribution at the runner outlet

Until now, the studies present in literature are only focused on the blades turbulent wakes evolution, especially in air flows and in axial flow machines. Earlier studies of basic test cases, like the flow behind a cylinder or step, provided a way to proceed with the analysis of more complex configurations, as the stay/guide vanes and runner blades in turbomachines.

Raj and Lakshminarayana (Ref 8] determined an analytical expression for the velocity defect decay on the turbulent wake centerline, based on *Townsend's* [Ref 7] model for the velocity and length scales and assuming the self-preservation of the mean velocity profile:

$$C_c/C_{\max} \propto (L/L_c)^{-(1-m)/2} \quad (1)$$

The turbulent wake of a cascade of airfoils is analyzed, from this point of view, for different incidences. Two distinct zones are observed in the turbulent wake behavior:

a near turbulent wake region, with rapid velocity decay – 70-80% to about half a blade chord distance downstream the trailing edge ($L/L_c > 0.5$), and $m > 0$ for adverse pressure gradients, in their case;

a far turbulent wake region, where the velocity defect decays much slower, but the form $C_o/C_{\max} \propto (L/L_c)^{-1}$ has not been verified for distances behind one chord downstream.

Zaccaria and Lakshminarayana [Ref 10] studied the rotor's turbulent wake of an axial aerodynamic turbine. Based on the *Schlichting's* [Ref 9] approach for a two-dimensional turbulent wake:

$$W_c/W_{\max} \propto (L/L_c)^{-1/2} \quad (2)$$

the following relation for the velocity defect variation in relative flow is found:

$$\frac{W_c}{W_{\max}} = 0.14 \left(\frac{Z}{L_{cax} \cdot \cos \beta_o} \right)^{-0.5} \quad (3)$$

The velocity variation is examined in the relative frame, with an approximation for the streamwise distance, assuming that the relative flow angle downstream the rotor doesn't vary and equals the blade angle at the trailing edge. The near turbulent wake region is estimated at only 20-30% of the chord length.

Lakshminarayana and Davino [Ref 6], in a study carried-out on the guide vanes and stator blades of an axial flow compressor analyzed the turbulent wake dissipation separately on each velocity component. It is concluded that the tangential and axial velocity defects match the general form:

$$C_c = a_1 \left(\frac{Z}{L_c} - z_o \right)^{-n+1} + a_2 \left(\frac{Z}{L_c} - z_o \right)^{-n} \quad (4)$$

The total velocity defect decay is found to follow a same expression. The tangential component decays slower than the axial one in the case of the stator, but it has almost the same decay rate for the guide vanes case. For the total velocity defect, 2 values of n are determined: 1.22 in the near turbulent wake region and 1.0 in the far turbulent wake region.

In all these studies, the wake centerline is supposed to evolve along a constant radius surface.

This paper aims to show that the sheared flow, generated by the uneven velocity distribution in the runner channel, follows the same decay law as the far wake of the blades. The analysis of the sheared flow transport/dissipation at the runner outlet in a Francis turbine draft tube cone is carried-out by an experimental study. A comparison with axial compressors is performed in order to quantify the runner blade-to-blade sheared flow dissipation law.

Experimental set-up

Turbine model

This study is part of the EUREKA project no.1625, FLINDT, Flow Investigation in Draft Tubes, whose aim is an efficient improvement of the draft tube performances through new design principles and tools, see *Avellan* [Ref 1].

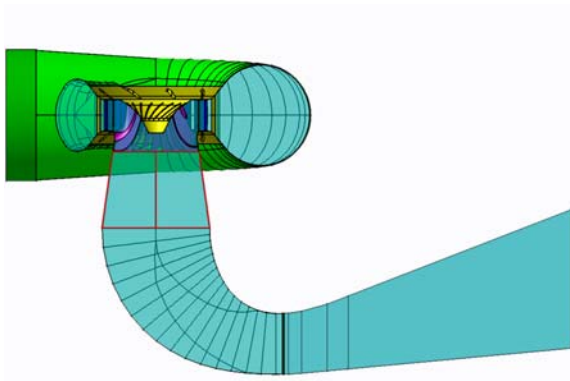


Figure 2 Turbine model

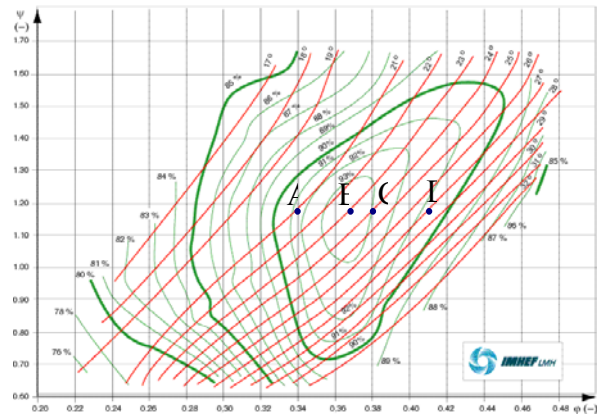


Figure 3 Operating points description by means of ϕ - ψ coefficients

The test model is a $n=0.56$ ($n_q=92$) Francis turbine, with 10 stay vanes, 20 guide vanes and 17 runner blades, see Figure 2. Four operating points are chosen on the turbine's characteristic chart for the same energy coefficient, $\psi=1.18$, and 4 discharge coefficients at: $0.92Q_{BEP}$, Q_{BEP} , $1.03Q_{BEP}$ and $1.11Q_{BEP}$, see Figure 3. The global measurements of discharge, specific energy and efficiency are performed according to IEC 60193 standards [Ref 11] at the Laboratory for Hydraulic Machines of EPFL.

Measurement zone

The flow field is investigated in a near-wall region of $130 \times 200 \text{ mm}^2$ area, in the middle longitudinal section of the cone, starting at 20% of the cone's height from the runner outlet and covering 20% of the median cone section area, see Figure 4.

3D-PIV

The 3D instantaneous velocity field in the cone is investigated with a Dantec 3D PIV system, which consists of a double-pulsed laser, 2 double-frame cameras and a processor unit for the acquisition synchronization and the vectors detection by cross-correlation.

The illuminating system is composed of 2 Nd:YAG laser units, each delivering a short impulse of 10 ns and 120 mJ energy at 8 Hz frequency. Thus the time interval between 2 successive impulses can easily be adjusted within 1 μs - 100 ms range, depending on the local flow characteristics or the phenomenon, which is to be captured. The output laser beam of 532 nm is guided through an optical arm, for accessibility, to a beam expander and transformed into a sheet of 4 mm width and 25° divergence.

Two Hi-Sense cameras with a resolution of $1'280 \times 1'024$ pixels are used for $130 \times 200 \text{ mm}^2$ area. The cameras are placed in a stereoscopic configuration, focused on the laser-sheet, synchronized with the two pulses, and they capture the position of glass seeding particles of $\sim 10 \mu\text{m}$ diameter, by detecting their scattered light.

For the optical access, the cone is manufactured in PPMA with a refractive index of 1.4, equipped with a narrow window for the laser's access and two large symmetric windows for the cameras access, having a flat external surface for minimizing the optical distortions.

The corresponding two-dimensional vector maps, obtained from each camera by an FFT-based algorithm, are combined in order to have the out-of-plane component, characterizing the displacement in the laser-sheet width.

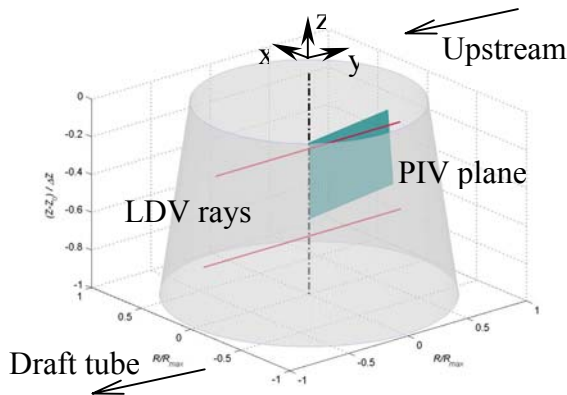


Figure 4 Definition of measurement sections and reference frame

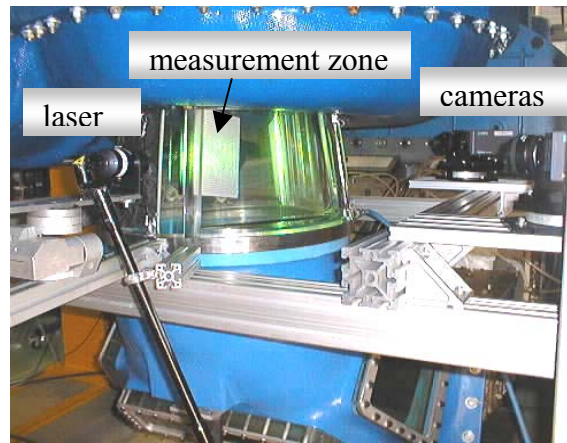


Figure 5 Calibration set-up for 3D PIV measurements

The correlation between the local image coordinates and real space coordinates is realized through a 3rd order optical transfer matrix, which includes the correction of distortions due to different refractive indices in the optical path and to the oblique position of the cameras. The calibration relation is obtained acquiring images of a plane target with equally spaced markers, moved in 5 transversal positions in order to have volume information, see Figure 5.

The target displacement in the measurement zone, with accuracy within the narrow limits of 0.01 mm in translation and 0.1° in rotation, insured a good calibration quality, see *Iliescu et al.* [Ref 4].

Measurement results

Data acquisition and post-processing

The spatial resolution of the vector fields in the measurement plane is 2.4x2.5 mm. Each raw instantaneous velocity field is filtered by means of the signal-to-noise ratio criteria and by a moving average algorithm.

For periodic flows, the signal can easily be reconstructed by synchronizing the acquisition with a reference signal at several time shifts τ , see Figure 6. The signal can be decomposed according to:

$$C_i(t) = \bar{C} + \tilde{C}(\tau) + C'(t) \quad (5)$$

The phase-locked component $\bar{C} + \tilde{C}$ is obtained by averaging the instantaneous values at the same τ value, see (8).

$$\bar{C} = \langle C_i \rangle = \lim_{N \rightarrow \infty} \frac{1}{N} \sum_{i=1}^N C_i(t) \quad (6)$$

$$\tilde{C}(\tau) = \lim_{N' \rightarrow \infty} \frac{1}{N'} \sum_{i=1}^{N'} (C_i(\tau) - \bar{C}) \quad (7)$$

with: $\bar{C} = 0$
 $\langle C' \rangle = \lim_{N \rightarrow \infty} (C_i(t) - \bar{C} - \tilde{C}) = 0$

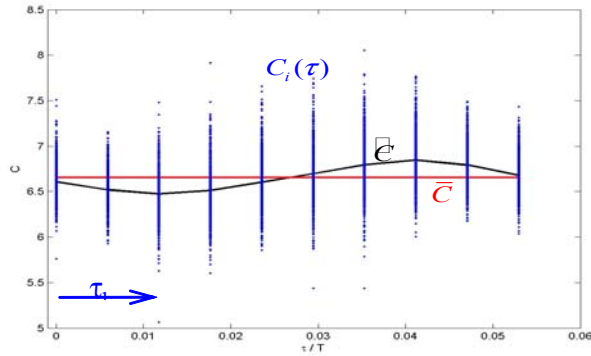


Figure 6 Phase average calculation of the velocity signal

Ten phase values, equidistant in a blade-to-blade interval, T_b , are selected to complete the phase average. Thus the blade-to-blade synchronous flow is reconstituted and, assuming the radial symmetry and multiplying by the number of blade passages, the flow over the entire runner rotation period T is determined, see (9).

$$T_b = \frac{T}{z_b} = \frac{1}{z_b f} = \frac{1}{f_b} \quad (8)$$

Subsequent to a mean convergence study, the number of acquired vector maps for each phase, τ value, has been set to 1'200, thus the mean velocity value \bar{C} represents the statistic over 12'000 instantaneous velocity fields.

The accuracy of the PIV measurements is 3% of the mean velocity value. The direct comparison with the LDV measurements in the upper part of the cone, see Figure 7 and *Iliescu et al.* [Ref 4], shows a good agreement.

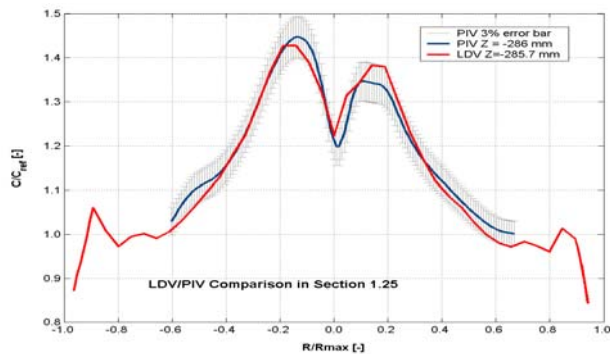


Figure Comparison LDV – PIV measurements

Results

The mean velocity field, \bar{C} , is reconstructed in the turbine cone for all operating points, see Figure 8.

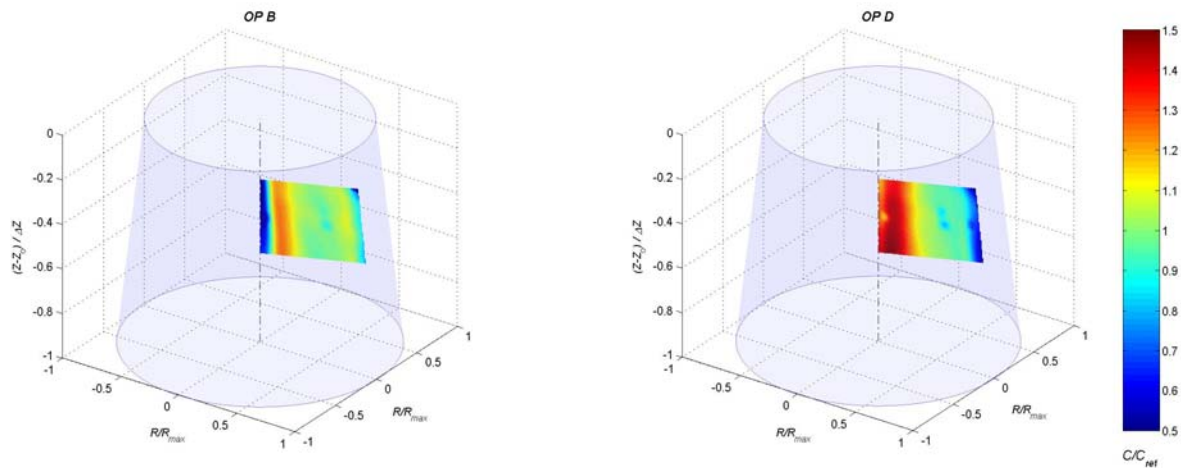


Figure 8 Mean velocity distribution in two operating conditions

By phase average, 10 velocity fields of the synchronous velocity component \tilde{C} are obtained for a blade-to-blade passage interval, see Figure 9.

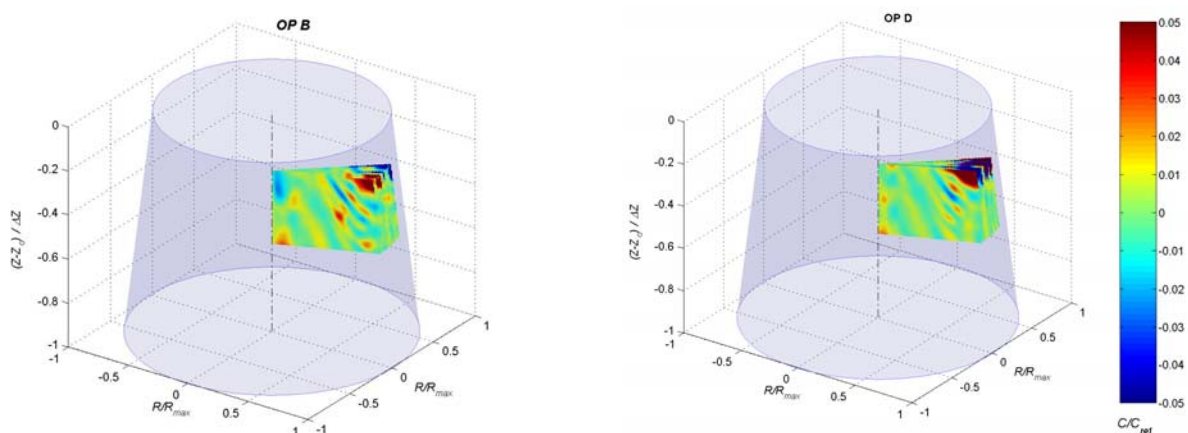


Figure 9 Phase average distribution in two operating conditions

For each PIV measurement point, in the same spatial position, the peak-to-peak fluctuation value is calculated starting from the PIV phase average results. For the LDV measurements, see Ciocan *et al.* [Ref 2], the synchronous velocity field in two sections, at 0.2 D and at 0.6 D cone depth, is reconstructed starting from the phase-average values. The results presented in Figure show that the maximum amplitude fluctuation, synchronous with the blade-to-blade passage, decreases from 15% of C_{ref} in the upper section of the cone at less than 1% at the cone exit.

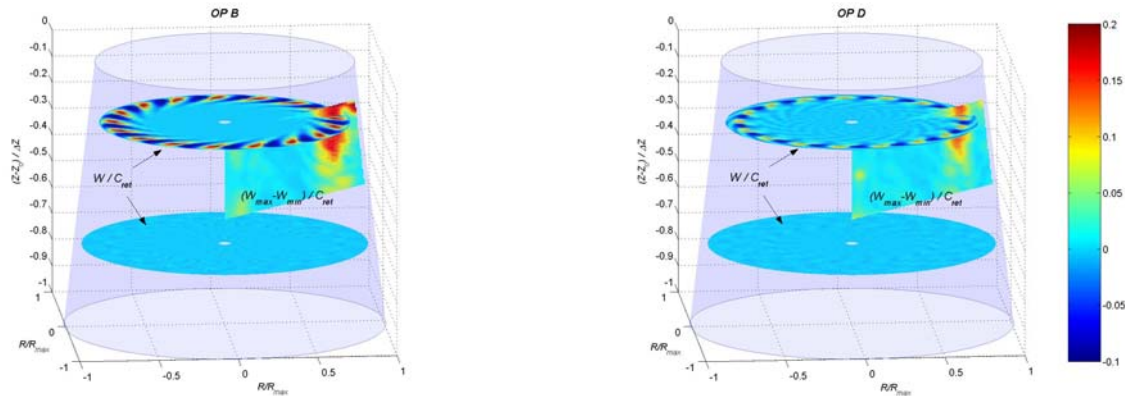


Figure 10 Amplitude of blade-to-blade phase average velocity for two operating points

Runner blade-to-blade sheared flow decay

The sheared flow incoming in the cone, originating from the uneven velocity distribution in the blade-to-blade channel, see Figure 1, has a turbulent wake-specific behavior and propagates downstream following the relative motion direction. The sheared flow trajectory could be followed in the absolute reference frame, in the same way as the trajectory of a fluid particle moving in a velocity field, which is given by its positions $X(R, \theta, Z)$ at each t moment, as solutions of the differential system:

$$\frac{d\vec{X}}{dt} = \vec{C}(\vec{X}, t) \quad (9)$$

Nevertheless, in the absolute reference frame, the flow is unsteady and we have not available unsteady velocity values in the whole volume to accurately describe the sheared flow dissipation trajectory. Spatially, PIV measurements provide only information in a plane, but assuming the flow periodicity and axi-symmetry in the cone, we can reconstruct the velocity field starting from the phase-averaged values of the relative velocity. Considered from the rotating frame of reference, the relative flow is steady, and the trajectory can be computed as a streamline given by:

$$\vec{dL} \times \vec{W} = 0 \quad (10)$$

The relative velocity W is described, in cylindrical coordinates, by its components in tangential, radial and axial directions:

$$W_u = C_u - U, \quad W_r = C_r, \quad W_z = C_z \quad (11)$$

The elementary length dL is defined, in cylindrical coordinates, by:

$$dL^2 = dR^2 + R^2 d\theta^2 + dZ^2 \quad (12)$$

Thus, the streamline path can be evaluated by integrating the following differential system:

$$\frac{dR}{W_r} = \frac{Rd\theta}{W_u} = \frac{dZ}{W_z} \quad (13)$$

In order to check that the sheared flow dissipates along the relative streamline, we identified the location of the maximum amplitude, corresponding to the maximum peak-to-peak value of the relative velocity fluctuation, in each plane of constant Z-coordinate, and we followed it in the entire volume, along the cone height, see Figure 11.

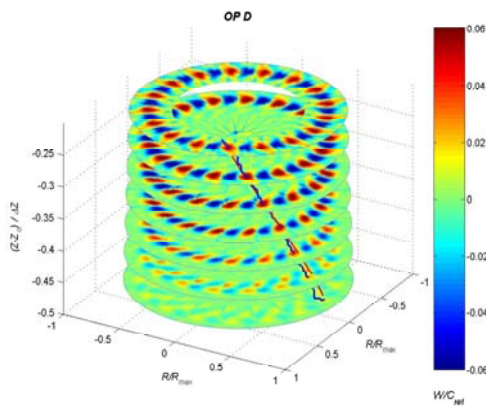


Figure 11 Path of maximum amplitude of the blade-to-blade phase average velocity

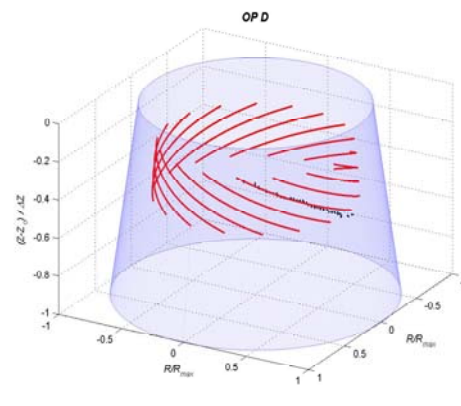


Figure 12 Path of streamlines (red) and maximum amplitude (black) of the blade-to-blade phase average velocity

Estimating the relative difference between the maximum amplitude path and streamline, see Figure 12, it can be observed that, for the significant part of the runner blade-to-blade sheared flow decay, our hypothesis is well adapted to the real case.

The phase-average values of the relative velocity for each depth, considered on the path of maximum amplitude and on the streamline, see Figure 13 and Figure 14, generate a conical surface and show a good agreement between these two calculations.

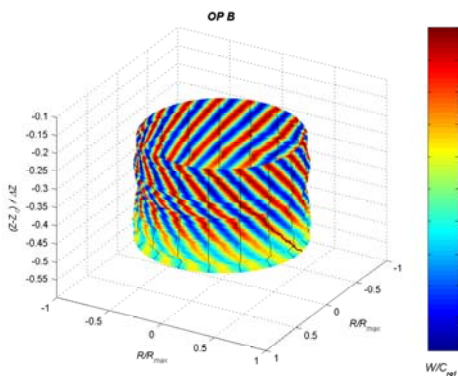


Figure 13 \tilde{W} over the path of max. amplitude

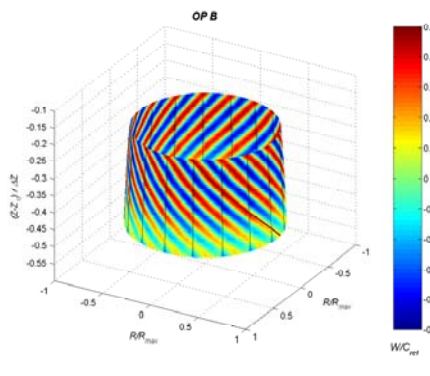


Figure 14 \tilde{W} over the streamline

In the static case, as the stator or guide vanes, authors like *Lakshminarayana and Davino* [Ref 6], neglected the path curvature, but, in the rotating blades case, the influence of swirl takes to the extension of the dissipation path onto several blade passing periods, T_b . This is clearly visible in Figure and Figure , where the black lines delimitate the blade-to-blade channels. *Zaccaria et al.* [Ref 10], in their study of an axial turbine rotor, estimated that the path curvature is induced by the relative flow angle at the blade trailing edge, and it remains constant downstream the rotor. This hypothesis is valid in the case of a cylindrical exit pipe, but is not true in the case of a cone, where the relative flow angle β decreases linearly downstream, see Figure 15.

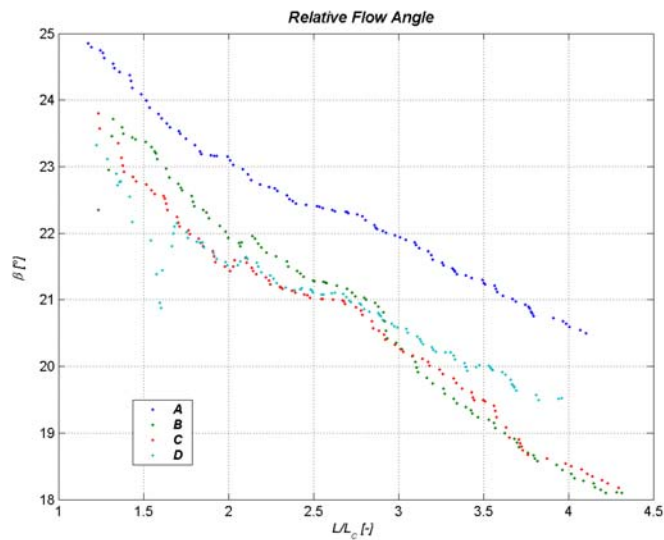


Figure 15 Influence of the discharge coefficient on the β relative flow angle distribution along the streamline

By following the *Schlichting's* [Ref 9] law for an axi-symmetric turbulent wake, with W and L on the measured maximum amplitude path or streamline path:

$$\frac{W}{C_{ref}} = a \left(\frac{L}{L_c} \right)^{-1} \quad (14)$$

a good approximation is obtained for the runner blade-to-blade sheared flow decay up to 3.5 chord lengths downstream, for the two path calculations, see Figure 16. This relation is in agreement with the result of *Raj and Lakshminarayana* [Ref 8] for a far wake.

The proportionality constant a is obtained for each operating point between 0.2 and 0.3, see Figure 17. Thus the runner blade-to-blade sheared flow decay, by turbulent mixing, is similar with the velocity decay on the centerline of a far turbulent wake.

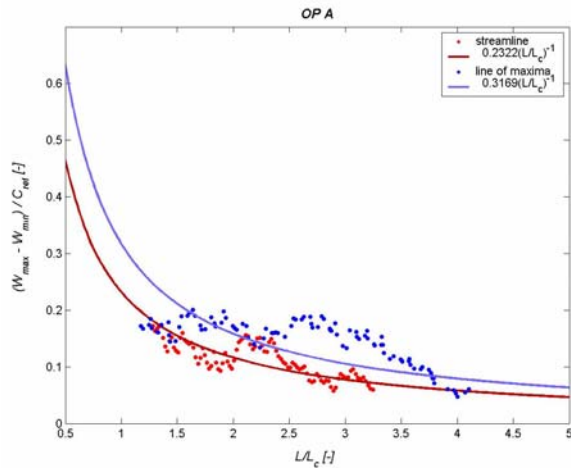


Figure 16 Velocity defect decay in relative reference frame along the streamline and along the maximum amplitude path

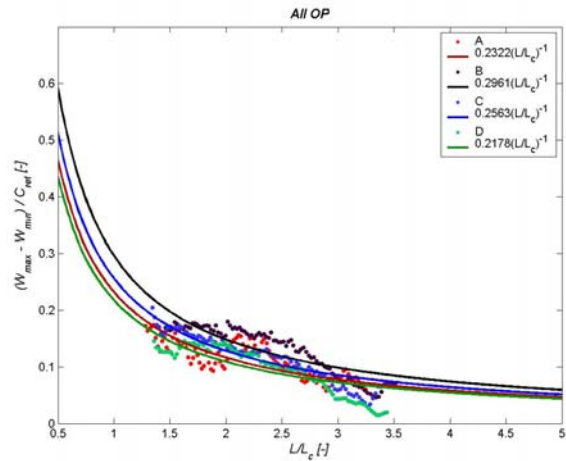


Figure 17 Velocity defect decay along the streamline in relative reference frame, for all operating points

The law (15) applied on the streamline approximates with a good accuracy, 5%, the velocity defect decay, i.e. the decrease of the peak-to-peak value of the runner blade-to-blade sheared flow in the turbine cone, see Figure 18. The previous LDV data, see Ciocan *et al.* [Ref 2], performed in only two cross-sections at the cone's inlet and outlet, were not sufficient for estimating the sheared flow velocity decay, but they integrate very well our model, fitting within the accuracy limits, see darker points in Figure 1.

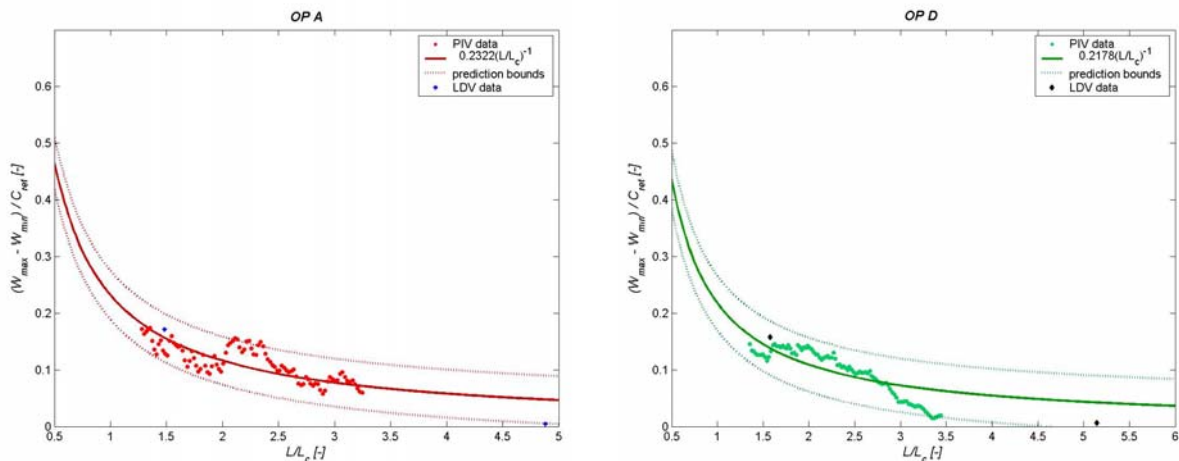


Figure 18 Velocity defect decay following the streamline in relative reference frame

Conclusions

The development of the incoming sheared flow in a draft tube cone of a scale model Francis turbine has been investigated with a 3D PIV technique. By phase averaging technique applied to the measured velocity field, the periodic component of the flow is extracted. Therefore, the runner blade-to-blade sheared flow structure can be emphasized and the mixing of the flow shearing is made apparent. A further analysis of the flow field in the rotating frame of

reference evidences that the runner blade-to-blade sheared flow mixing is similar to the dissipation of a far turbulent wake as described by *Schlichting*. The complete streamwise mixing of the flow can be considered as achieved, defect velocity of less than 2% of the C_{ref} , over a streamline length corresponding to 3.5 chord lengths.

Acknowledgements

The authors would like to thank particularly all the partners of the FLINDT II Eureka Project No 1625, i. e. ALSTOM Hydro, EDF-CIH, GE Hydro, VA TECH Hydro, VOITH-SIEMENS Hydro Power Generation for their financial support and assistance. The FLINDT II project is funded by PSEL, Funds for Projects and Studies of the Swiss Electric Utilities, Contract award No 126, and CTI, Swiss Federal Commission for Technology and Innovation, Contract award No 5190.2 EUS. The authors would like also to thank gratefully the staff members of the EPFL Laboratory Hydraulic Machines, for their technical assistance.

References

- Ref 1 Avellan F., "Flow Investigation in a Francis Draft Tube: the Flindt Project", *Proceedings of the 20th IAHR Symposium, August 7-9 2000*, Charlotte, North Carolina, USA
- Ref 2 Ciocan G.D., Avellan F., Kueny J.L. "Optical Measurement Techniques for Experimental Analysis of Hydraulic Turbines Rotor-Stator Interaction" - *ASME Fluid Engineering Conference*, 11-15 June 2000, Boston, USA
- Ref 3 Ciocan G.D., Mauri S., Arpe J., Kueny J.L., "The Experimental and Numerical Study of the non stationary velocity field at the exit of a turbine runner" *La Houille Blanche* no. 2, 2001
- Ref 4 Iliescu M.S., Ciocan G.D., Avellan F. "3D PIV and LDV Measurements at the Outlet of a Francis Turbine Draft Tube", *FEDSM2002-31332, Joint US ASME – European Fluids Engineering Summer Conference*, Montreal, Quebec, Canada, July 14-18, 2002
- Ref 5 Iliescu M.S., Ciocan G.D., Avellan F. "2 Phase PIV Measurements at the Runner Outlet in a Francis Turbine", *FEDSM2003-45756, Joint US ASME – European Fluids Engineering Summer Conference*, Honolulu, Hawaii, USA, July 6-10, 2003
- Ref 6 Lakshminarayana, B. Davino, R., 1980, "Mean Velocity Characteristics of the Guidevane and Stator Blade Wake in an Axial Flow Compressor", *Journal of Engineering for Power, Vol. 102, pp 485-493*, January 1980
- Ref 7 Townsend A.A., "The Structure of Turbulent Shear Flow", *Cambridge University Press*, 1976
- Ref 8 Raj R., Lakshminarayana, B., "Characteristics of the wake behind a cascade of airfoils", *Journal of Fluid Mechanics, vol. 61, part 4, pg. 707-730*, 1973
- Ref 9 Schlichting, H., "Boundary-Layer Theory", *Mc GRAW-HILL BOOK Company, New York*, 1968

Ref 10 Zaccaria M.A., Lakshminarayana, B., “Unsteady flow field due to nozzle wake interaction with the rotor in an axial flow turbine: part 2 Rotor exit flow field”, *Journal of turbomachinery*, vol. 119, pg. 214-224, April 1997

Ref 11 IEC 60193, "Model acceptance tests to determinate the hydraulic performance of hydraulic turbines, storage pumps and pump-turbines", *International Standard I.E.C.*, 1993